Baroclinically Unstable Geostrophic Turbulence in the Limits of Strong and Weak Bottom Ekman Friction: Application to Midocean Eddies

BRIAN K. ARBIC*

MIT–WHOI Joint Program in Oceanography, Massachusetts Institute of Technology, Cambridge, and Woods Hole Oceanographic Institution, Woods Hole, Massachusetts

GLENN R. FLIERL

Program in Atmospheres, Oceans, and Climate, Department of Earth and Planetary Sciences, Massachusetts Institute of Technology, Cambridge, Massachusetts

(Manuscript received 4 August 2003, in final form 24 February 2004)

ABSTRACT

This paper examines the plausibility of mesoscale eddy generation through local baroclinic instability of weak midocean gyre flows. The main tool is a statistically steady, two-layer quasigeostrophic turbulence model driven by an imposed, horizontally homogeneous, vertically sheared mean flow and dissipated by bottom Ekman friction. A wide range of friction strengths is investigated. In the weakly damped limit, flow is nearly barotropic, and the horizontal length scale of barotropic energy increases with decreasing friction, consistent with previous studies. The strongly damped limit, explored here for the first time, is equivalent barotropic (lower-layer velocities are nearly zero) and features an increase in the horizontal scale of potential energy with increasing friction. Current-meter data suggest that midocean eddies lie between the barotropic and equivalent barotropic limits. In accord with this suggestion, the moderately damped regime of the model compares well to observations of eddy amplitude, vertical structure, and horizontal scale, especially when stratification is surface intensified. A review of pertinent observations suggests that mesoscale eddies may indeed lie in the moderately damped limit. These arguments are first developed in f-plane simulations. Previous studies of beta-plane turbulence have had eastward mean flows, and in this case eddy energy has little sensitivity to friction. However, midocean gyre flows are generally nonzonal, and this nonzonality appears to be a significant factor in the production of energetic eddies. Beta-plane turbulence driven by nonzonal mean flows is sensitive to bottom friction, such that moderate damping is required for model eddies to compare well to observations, as on the f plane. A heuristic argument is presented in support of this similarity.

1. Introduction

This paper discusses part of our investigation (Arbic 2000) into the plausibility of baroclinic instability of weak midocean gyre flows as a generation mechanism for midocean eddies. Here we ask whether baroclinically unstable quasigeostrophic (QG) turbulence can have eddy kinetic energies larger than that of the mean while retaining substantial kinetic energy in the baroclinic mode and in length scales near the first-baroclinic-mode deformation radius (L_d). Midocean eddies meet these criteria, but previously published flat-bottom QG turbulence simulations, working in the freely decaying and weakly damped limits, have undergone an inverse cascade to large-scale barotropic flow. We will argue that moderately strong bottom friction, coupled with surface-intensified stratification, can arrest the inverse cascade.

In the midlatitude midocean, time-varying geostrophic motions such as rings, Rossby waves, and mesoscale eddies have one to two orders of magnitude more kinetic energy than the time-mean circulation (cf. Gill et al. 1974; Wunsch 2001). Quantifying the various sources of eddies remains a matter of ongoing research. Energies are highest in boundary currents (cf. Schmitz 1996a,b and references therein; Stammer 1997) reflecting meandering (cf. Maul et al. 1978), the generation of rings (cf. Cheney and Richardson 1976; Richardson 1983), and the production and radiation of Rossby waves (cf. Flierl and Kamenkovich 1975; Talley 1983; Hogg 1988; Chester et al. 1994; Kamenkovich and Pedlosky 1996). Thus, nonlocal generation of midocean eddies in boundary currents is undoubtedly significant, but local sources also play a role. Float data sometimes show eddies spontaneously arising in the interior (O. Boebel 2000, per-

* Current affiliation: Program in Atmospheric and Oceanic Sciences, Princeton University/GFDL, Princeton, New Jersey.

Corresponding author address: Dr. Brian K. Arbic, Program in Atmospheric and Oceanic Sciences, Princeton University/GFDL, P.O. Box CN710, Sayre Hall, Princeton, NJ 08544-0710.
E-mail: arbic@splash.princeton.edu

sonal communication). Direct generation of eddies by fluctuating winds was proposed by Frankignoul and Müller (1979) and Müller and Frankignoul (1981), and further investigated by Treguier and Hua (1987, 1988) and Large et. al. (1991). Stammer and Wunsch (1999) found significant correlations at high latitudes between observed temporal variations in eddy kinetic energy and in wind stress. However, these correlations explain only some of the eddy energy and are even smaller at low latitudes.

Midocean baroclinic instability (Gill et al. 1974; Robinson and McWilliams 1974) is another potential source of eddy formation. Hogg (1985) found that observed eddy characteristics in the Gulf Stream recirculation region (zonal phase propagation, horizontal scales, and vertical phase shifts) resemble predictions from linear baroclinic instability theory (Charney 1947; Eady 1949). Gill et al. (1974) demonstrated that the large-scale circulation stores more than enough potential energy to produce the observed eddy kinetic energies. Stammer (1997) showed that eddy velocities are well correlated with mean thermal wind velocities. Such evidence suggests that local baroclinic instability does contribute importantly to the generation and maintenance of the eddy field.

Agreement between the data and nonlinear theory is less clear. Nonlinear interactions in freely decaying two-dimensional turbulence effect a cascade of energy toward large horizontal scales (Batchelor 1953; Fjortoft 1953). If this inverse cascade were fully developed in the midocean, eddies would be at basin scales. Instead, they are much more compact. Rhines (1975) showed that freely decaying turbulence stops cascading at a scale $\sqrt{U/\beta}$, where U is an eddy velocity scale and β is planetary beta. The arrest scale arises from a balance between advective and Rossby wave phase speeds. However, the latter are of order 2 cm s^{-1}, one-fifth of typical eddy swirl speeds (MODE Group 1978). Eddy horizontal scales correlate better with L_d than with $\sqrt{U/\beta}$ over the wide range of latitudes covered by altimetric data (Stammer 1997). Predictions of vertical structure are likewise questionable. Charney (1971) and Rhines (1977) showed that freely decaying stratified QG turbulence undergoes an inverse cascade to the barotropic mode as well as to large horizontal scales. Similar effects have been found in weakly damped baroclinically unstable turbulence (cf. Salmon 1978, 1980; Larichev and Held 1995). However, current-meter data (cf. Wunsch 1997 and references therein) indicate that in most locations the first baroclinic mode contains a substantial fraction of eddy kinetic energy.

Our study uses a two-layer, doubly periodic, rigid-lid QG turbulence model forced by an imposed, horizontally homogeneous, vertically sheared mean flow and dissipated by bottom Ekman friction. The model is meant to represent a patch of an ocean gyre, large enough to contain many eddy lengths but small enough so that the mean flow varies slowly in space. The imposed shear is assumed to be generated by wind and buoyancy forcing, and altered by other processes that do not appear explicitly in the model, for instance, eddy flux divergences. Similar models have been used by Salmon (1978, 1980), Haidvogel and Held (1980), Vallis (1983), Hua and Haidvogel (1986), Panetta (1993), Larichev and Held (1995), Held and Larichev (1996), Smith and Vallis (2002), and Lapeyre and Held (2003).

Although previous papers on baroclinically unstable QG turbulence have noted a model sensitivity to bottom Ekman friction (cf. Larichev and Held 1995), few have made this sensitivity a primary focus, as we do here. Several papers (cf. Williams and Robinson 1974; Pedlosky 1983; Riviere and Klein 1997; and others) have explored the sensitivity of linear or weakly nonlinear systems to friction. Smith et al. (2002) and Riviere et al. (2004) describe an increase of horizontal eddy length scales with decreasing friction. The former studied one-layer QG forced–dissipated turbulence; the latter studied multilayer turbulence driven by inhomogeneous background flows, in both primitive equation and QG simulations. We will vary friction strength by a factor of 2000, a far greater range than in any previous study [e.g., Smith and Vallis (2002) and Riviere et al. (2004) varied friction by factors of 7 and 8, respectively, and both explored only the weakly damped limit]. We investigate the strongly damped limit, which has been explored only in Arbic and Flierl (2003) and here, as well as the moderately and weakly damped limits. Under strong damping, lower-layer velocities are nearly zero—the model state is equivalent barotropic. Under weak damping, lower-layer velocities are nearly as large as upper-layer velocities—the model state is barotropic. Midocean eddies appear to lie in between the equivalent barotropic and barotropic limits. Figure 2 of Colin de Verdiére et al. (1989) indicates that eddy structures remain remarkably similar with varying depth (suggesting the barotropic paradigm), but that amplitude decreases substantially (suggesting the equivalent barotropic paradigm). Thus the strongly damped regime is worthy of study not because the ocean necessarily lies there, but because the strongly and weakly damped regimes are asymptotic limits, which can be used to explain the properties of moderately damped turbulence. As we will show, moderately damped turbulence matches observations of midocean eddies best, especially when stratification is surface intensified. Our experiments examine the effects of stratification by contrasting experiments having thin upper layers with experiments in which the upper- and lower-layer depths are equal.

Both freely decaying turbulence (Rhines 1975) and baroclinically unstable turbulence driven by eastward mean flows (Panetta 1993; Held and Larichev 1996; Smith and Vallis 2002) are profoundly affected by β. Midocean mean flows generally have a significant meridional component. Motivated by this, Arbic and Flierl (2004) examined horizontally homogeneous beta-plane QG turbulence forced by nonzonal mean flows. If mid-

ocean mean flows were zonal, they are weak enough that they might be unable to generate energetic eddies in the face of realistic β values. However, even weak nonzonal flows can generate substantial eddy energy. We will present a heuristic argument that beta-plane turbulence driven by nonzonal mean flows should resemble f-plane turbulence. For simplicity, therefore, we first examine the sensitivity to friction in f-plane flow. Then we will show that a similar sensitivity exists in beta-plane turbulence driven by nonzonal mean flows.

2. The model

We introduce the model in its f-plane formulation, with governing equations

$$\frac{\partial q_1}{\partial t} + \overline{u_1}\frac{\partial q_1}{\partial x} + \frac{\partial \overline{q_1}}{\partial y}\frac{\partial \psi_1}{\partial x} + J(\psi_1, q_1) = \text{ssd} \quad \text{and} \tag{1}$$

$$\frac{\partial q_2}{\partial t} + \overline{u_2}\frac{\partial q_2}{\partial x} + \frac{\partial \overline{q_2}}{\partial y}\frac{\partial \psi_2}{\partial x} + J(\psi_2, q_2) = -R_2\nabla^2\psi_2 + \text{ssd}, \tag{2}$$

where $J(A, B) = \partial A/\partial x\, \partial B/\partial y - \partial A/\partial y\, \partial B/\partial x$, overbars denote imposed time-mean quantities, quantities without overbars denote fluctuations from the mean, u (v) denotes zonal (meridional) velocity, the subscript 1 (2) denotes upper (lower) layer, ssd denotes small-scale dissipation, and potential vorticity (PV; also q) is the prognostic variable. We have taken the mean flow to be zonal, but the f plane is rotationally invariant. The fluctuating streamfunctions ψ_1 and ψ_2 satisfy

$$q_1 = \nabla^2\psi_1 + \frac{(\psi_2 - \psi_1)}{(1 + \delta)L_d^2} \quad \text{and}$$

$$q_2 = \nabla^2\psi_2 + \frac{\delta(\psi_1 - \psi_2)}{(1 + \delta)L_d^2}, \tag{3}$$

where δ is the ratio H_1/H_2 of upper- to lower-layer depths and the deformation radius L_d is defined as in Flierl (1978) and Arbic and Flierl (2003, 2004). The fluctuating velocities are

$$(u_1, v_1) = \left(-\frac{\partial\psi_1}{\partial y}, \frac{\partial\psi_1}{\partial x}\right) \quad \text{and} \quad (u_2, v_2) = \left(-\frac{\partial\psi_2}{\partial y}, \frac{\partial\psi_2}{\partial x}\right). \tag{4}$$

The imposed mean PV gradients are

$$\frac{\partial \overline{q_1}}{\partial y} = \frac{(\overline{u_1} - \overline{u_2})}{(1 + \delta)L_d^2} \quad \text{and} \quad \frac{\partial \overline{q_2}}{\partial y} = \frac{\delta(\overline{u_2} - \overline{u_1})}{(1 + \delta)L_d^2}. \tag{5}$$

The bottom boundary layer thickness d_{Ekman} determines R_2 by

$$R_2 = \frac{f_0 d_{\text{Ekman}}}{2H_2}, \tag{6}$$

where f_0 is the Coriolis parameter (cf. Pedlosky 1987). Barotropic (BT) and baroclinic (BC) modes are defined as in Flierl (1978):

$$\psi_{\text{BT}} = \frac{\delta\psi_1 + \psi_2}{1 + \delta}, \qquad \psi_{\text{BC}} = \frac{\sqrt{\delta}(\psi_1 - \psi_2)}{1 + \delta},$$

$$q_{\text{BT}} = \frac{\delta q_1 + q_2}{1 + \delta} = \nabla^2\psi_{\text{BT}}, \quad \text{and}$$

$$q_{\text{BC}} = \frac{\sqrt{\delta}(q_1 - q_2)}{1 + \delta} = \nabla^2\psi_{\text{BC}} - \frac{1}{L_d^2}\psi_{\text{BC}}. \tag{7}$$

The barotropic mode represents depth-averaged flow. The baroclinic mode represents the depth-varying part of the flow, which has an associated horizontal scale L_d.

The total energy equation (Charney 1971) in layer form is

$$\frac{\partial}{\partial t}\iint \frac{1}{2}\left[\frac{\delta(\nabla\psi_1)^2}{1 + \delta} + \frac{(\nabla\psi_2)^2}{1 + \delta} + \frac{\delta(\psi_1 - \psi_2)^2}{(1 + \delta)^2 L_d^2}\right] dx\, dy - \frac{\delta(\overline{u_1} - \overline{u_2})}{(1 + \delta)^2 L_d^2}\iint \psi_1\frac{\partial\psi_2}{\partial x}\, dx\, dy = -\frac{R_2}{1 + \delta}\iint (\nabla\psi_2)^2\, dx\, dy + \text{ssd} \tag{8}$$

and in modal form is

$$\frac{\partial}{\partial t}\iint \frac{1}{2}\left[(\nabla\psi_{\text{BT}})^2 + (\nabla\psi_{\text{BC}})^2 + \frac{\psi_{\text{BC}}^2}{L_d^2}\right] dx\, dy + \frac{\sqrt{\delta}(\overline{u_1} - \overline{u_2})}{1 + \delta}\iint \left(q_{\text{BC}}\frac{\partial\psi_{\text{BT}}}{\partial x} + q_{\text{BT}}\frac{\partial\psi_{\text{BC}}}{\partial x}\right) dx\, dy = -\left(\frac{R_2}{1 + \delta}\right)\iint (\nabla\psi_{\text{BT}})^2\, dx\, dy - \left(\frac{\delta R_2}{1 + \delta}\right)\iint (\nabla\psi_{\text{BC}})^2\, dx\, dy + \frac{2\sqrt{\delta}R_2}{1 + \delta}\iint \nabla\psi_{\text{BT}}\cdot\nabla\psi_{\text{BC}}\, dx\, dy + \text{ssd}. \tag{9}$$

Densities of barotropic kinetic energy (KE_{BT}), baroclinic kinetic energy (KE_{BC}), and available potential energy (APE) are $(\nabla\psi_{\text{BT}})^2/2$, $(\nabla\psi_{\text{BC}})^2/2$, and $(\psi_{\text{BC}})^2/2L_d^2$, respectively. Motion in both layers, and in both modes, is required to generate energy (and enstrophy).

If we ignore ssd, the system is governed by two nondimensional parameters: δ and $(\overline{u_1} - \overline{u_2})/R_2 L_d$. We call the second one, which is the inverse of the $\hat{R}$ parameter in Riviere et al. (2004), "throughput."[1] We set $\overline{u_1} - \overline{u_2}$ to 1 cm s^{-1}, a typical midocean value in altimetric

[1] We thank J. McWilliams for suggesting this name. It evokes an image of eddies growing from the mean flow and then being dissipated by bottom friction. In the strongly damped (low throughput) limit, bottom friction controls the eddies, while in the high-throughput limit eddies turn over many times before feeling bottom friction.

data (Wunsch 2001), current-meter data (cf. Müller and Siedler 1992), and hydrographic data (cf. Fig. 4 of Stammer 1997). We set L_d to 50 km, a common value in subtropical gyres (cf. Richman 1976; Stammer 1997). The model domain size is $20\pi L_d$, or 3142 km. A much larger domain no longer plausibly represents a patch of a gyre. Our domain is smaller by a factor of 5 than that of Larichev and Held (1995), who left more room for the inverse cascade to proceed. We resolve activity near L_d better with our smaller domain. All of the results in this paper represent domain and time averages after equilibration was reached in 256 squared simulations. Experiments were initialized with fields randomly generated in physical space. Except where noted, plots are of nondimensional quantities. Energies are normalized by $[(\overline{u_1} - \overline{u_2})^2]/2$, and streamfunctions by $(\overline{u_1} - \overline{u_2})L_d$. Our numerical model is pseudospectral. All of the experiments in the present paper use an exponential cutoff wavenumber filter for ssd. Details of the model numerics and wavenumber filter are in Arbic (2000) and Arbic and Flierl (2003, 2004). Our preference for a filter stems from experiments in LaCasce (1996), which showed that the filter preserves the shape and amplitude of propagating modons much better than does hyperviscosity or Laplacian friction. As shown by the rightmost points of Figs. 4b and 5b in Arbic and Flierl (2004), eddy statistics in the order-1 throughput regime of greatest interest in the present paper appear to be relatively unaffected by the choice of small-scale dissipation.[2] To the best of our knowledge, the lattice vortex regime of Arbic and Flierl (2004) is the only regime in our papers that is strongly affected.

3. Friction strength in the ocean

To evaluate throughput we must estimate R_2 for the midlatitude midocean. Potentially, R_2 could be a proxy for unresolved processes other than bottom Ekman layers—for instance, flow interactions with rough topography. Let us first assume that R_2 represents boundary layer physics. Weatherly and Martin (1978) measured bottom boundary layer depths to be about 10 m. Inserting this into (6) along with $H_2 = 4000$ m and $f_0 = 10^{-4}$ s^{-1} yields a decay rate of (100 days)$^{-1}$. In ocean general circulation models, a link is often made between assumed background tidal flows (unresolved in the model) and quadratic bottom boundary layers. The widely used 0.0025 value of the quadratic drag coefficient then implies an order (150 days)$^{-1}$ decay rate—see discussions in Willebrand et al. (2001) and Riviere et al. (2004). Order (100 days)$^{-1}$ decay rates are consistent with those ascertained from current-meter data for the barotropic mode (Wunsch 1998). Gille et al. (2000) inferred from altimetry data a surface eddy decay time of 550–1450 days. Much of the surface eddy kinetic energy is in the baroclinic mode. From (9) we see that the baroclinic mode decays one-fifth as fast as the barotropic mode when $\delta = 0.2$, a value representative of surface-intensified stratification (Fu and Flierl 1980). To complement this argument, which suffers from the presence of the sign-indefinite $\nabla\psi_{\rm BT} \cdot \nabla\psi_{\rm BC}$ term in (9), we perform a two-layer version of the linear analysis done for Rossby wave decay in the continuously stratified case (Charney and Flierl 1981). We find that baroclinic waves decay at rates $\delta K^2/(K^2 + 1/L_d^2)$ times the decay rate of barotropic waves, where K is the total wavenumber. If we assume that $K \sim 1/L_d$, we again infer an order δ difference in decay rates between the two modes. If we assume Gille et al.'s decay time represents that of the baroclinic mode, then R_2, the decay rate of the barotropic mode, may lie between (100–300 days)$^{-1}$. A throughput value of 2.5 corresponds to a decay rate of (145 days).$^{-1}$ We shall denote the $\delta = 0.2$, throughput $= 2.5$ experiment by 0.2/2.5, and we assume it to be representative of the midocean. Gulf Stream rings can survive for a few years, but this does not necessarily mean that decay times are this long, because the rings may be extracting energy from the background mean flow to balance dissipation. In the lattice vortex regime of Arbic and Flierl (2004), individual coherent vortices persist indefinitely in the presence of friction by extracting energy from a baroclinically unstable mean flow.

Clearly, our estimate of throughput is rough. Mean flows in some midocean regions are larger than 1 cm s^{-1}, and the deformation radius is much less than 50 km in high latitudes. Furthermore, two-layer models may underestimate shear, since they do not resolve vertical structure within the thermocline. Accounting for these factors may increase throughput significantly. However, some studies suggest at least the possibility that our (145 day)$^{-1}$ friction estimate may be too weak. Egbert and Ray (2001) found that about 1 TW of tidal dissipation (mostly at semidiurnal frequencies) takes place in the midocean. The 0.0025 quadratic drag value is two orders of magnitude too small to account for this midocean tidal dissipation (Munk 1997; Jayne and St. Laurent 2001). Instead midocean tidal dissipation is almost certainly dominated by the generation and subsequent breaking of internal waves as tidal flows interact with rough topography (Polzin et al. 1997; Egbert and Ray 2001). Recent forward models of tides (Jayne and St. Laurent 2001; Arbic et al. 2004) parameterize the topographic drag and find that it must be quite strong to accurately simulate open-ocean tidal elevations. Arbic et al. (2004) find that globally averaged decay rates in the optimally tuned solutions in both of these studies are (2 days)$^{-1}$. Gille et al. (2000) found that eddy energies tend to be lower in regions of rough topography.

[2] The total eddy energy of the *f*-plane throughput = 3.33 "filter" experiment in Fig 5b of Arbic and Flierl (2004) is 10% higher than the total eddy energy of the *f*-plane throughput = 3.33 "hyper" experiment. Because of a mistake in plotting, the energy of the *f*-plane filter data point shown in the indicated figure is too low by a factor of 2.

Although the dynamics will be somewhat different from those involving semidiurnal tides, because of the lower frequencies involved, wind-driven motions are also likely to generate breaking internal waves as they flow over rough topography. We therefore ask whether similarly strong decay rates may apply to wind-driven motions. Indeed, Hirose et al. (2001) found that the maximum amount of observed TOPEX/Poseidon sea surface height variance they could explain in their model of wind-driven barotropic motions was achieved when spatially averaged bottom friction decay rates were of order $(2\ \text{days})^{-1}$. It is possible of course that this strong decay rate does not apply to mesoscale eddies, and it may be implausibly strong for use in ocean general circulation models. We conclude that the value of throughput is uncertain, but that it may be of order 1. We retain 2.5 as our nominal value, although the caveats outlined in this section should be kept in mind.

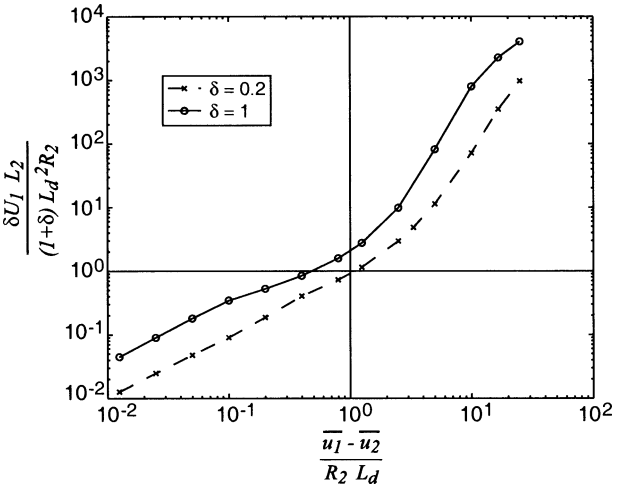

FIG. 1. Estimated ratios of nonlinear to Ekman friction terms (y axis) vs throughput (x axis) in the lower layer of the f-plane experiments ($\delta = 0.2$ and 1). The vertical line indicates a throughput of 1.

4. f-plane experiments

a. Surface-intensified versus uniform stratification

The baroclinic self-interaction term $J(\psi_{\text{BC}}, q_{\text{BC}})$ projects onto the baroclinic PV equation (not shown) if and only if layer depths are unequal (Flierl 1978). Fu and Flierl (1980) computed the projection of the square of the first baroclinic mode onto itself given a typical midlatitude stratification profile. This projection retains the same strength in the two-layer case when $\delta = 0.2$, which we take to represent surface-intensified stratification in midlatitudes (0.2 may not be an optimal value for all latitudes). We perform contrasting experiments with $\delta = 1$, which represents a uniform stratification. As anticipated by Flierl (1978) and Fu and Flierl (1980), Smith and Vallis (2001; also Arbic 2000) showed that the cascade to the barotropic mode in freely decaying stratified turbulence is weaker with surface-intensified stratification. As we shall see, in baroclinically unstable turbulence, eddy baroclinicity is controlled by bottom friction, with stratification playing a role unrelated to the above mechanism.

b. Spinup and equilibration

Our criterion for equilibration is that no trend be apparent in eddy energy, over a period at least as long as the spinup time. In all experiments an irregular temporal variability in eddy energy is seen after equilibration is reached, as in other turbulence studies (cf. Larichev and Held 1995). This contrasts with the quasi-periodic oscillations seen in weakly nonlinear systems (Pedlosky 1983). After equilibration is achieved, Ekman friction balances energy production to within 3% or better in all of the f-plane experiments. The wavenumber filter accounts for the rest of the dissipation. Since strong friction and large velocities both force model time steps to be small for numerical stability, experiments in both the strongly and weakly damped regimes are computationally expensive.

c. Model behavior in the strongly and weakly damped limits

We begin with a scaling of the strength of nonlinearity $J(\psi_2, q_2)$ relative to the strength of bottom friction in the lower-layer PV equation (2):

$$\frac{\text{Nonlinear term}}{\text{Ekman friction}} = \frac{J\left[\psi_2, \nabla^2\psi_2 + \dfrac{\delta(\psi_1 - \psi_2)}{(1+\delta)L_d^2}\right]}{R_2\nabla^2\psi_2} \sim \frac{J\left[\psi_2, \dfrac{\delta\psi_1}{(1+\delta)L_d^2}\right]}{R_2\nabla^2\psi_2} \sim \frac{\delta U_1 L_2}{(1+\delta)L_d^2 R_2}, \tag{10}$$

where U_1 is the time- and domain-averaged rms upper-layer eddy velocity, L_2 is the time- and domain-averaged lower-layer length scale, and the ψ_2 terms in q_2 are neglected because of the relative weakness of lower-layer motions. Note that (10) is a scale relation—an exact domain integral of the Jacobian vanishes under periodic boundary conditions. The ratio in (10) is plotted versus throughput in Fig. 1. When throughput is larger (smaller) than 1, nonlinear terms dominate over (are dominated by) friction in the lower layer. Throughput thus determines whether nonlinearities are strong enough in the bottom layer for it to participate in the inverse cascade. In the weakly damped (high throughput) limit, both layers experience an inverse cascade, and we therefore call this the barotropic limit. In the

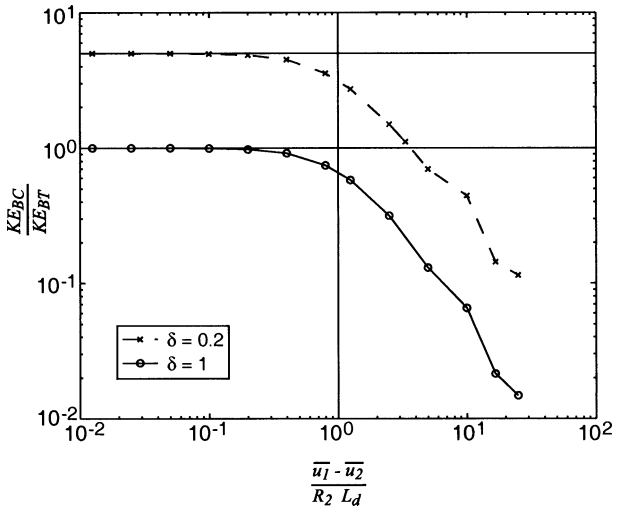

FIG. 2. Ratios of modal kinetic energies vs throughput in the f-plane experiments ($\delta = 0.2$ and 1). Horizontal lines indicate the limiting values of H_2/H_1.

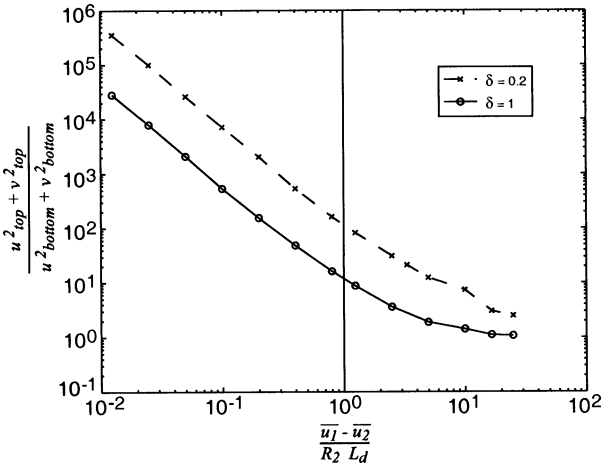

FIG. 3. Ratios of upper- to lower-layer squared velocities vs throughput in the f-plane experiments ($\delta = 0.2$ and 1).

strongly damped (low throughput) limit, only the upper-layer experiences an inverse cascade, and we therefore term this the equivalent barotropic limit. This dichotomy is of central importance to our paper.

Vertical structure is quantified in Figs. 2 and 3, which show ratios of baroclinic to barotropic kinetic energy and ratios of upper- to lower-layer squared velocities, respectively, versus throughput. When throughput exceeds 1, the system becomes increasingly barotropic (the baroclinic-to-barotropic-kinetic-energy ratio is much less than 1, and the layer velocities are nearly equal) as friction decreases. The system becomes more barotropic with decreasing friction just as freely decaying stratified turbulence becomes more barotropic with time (Rhines 1977). When throughput is less than 1, the ratio of upper- to lower-layer squared velocities becomes ever larger as friction increases. In this limit it is appropriate to set ψ_2 to zero in (7), which yields $\psi_{BC} = \psi_{BT}/\sqrt{\delta}$ and $KE_{BC}/KE_{BT} = H_2/H_1$. Figure 2 indicates that H_2/H_1 apparently serves as an upper bound on KE_{BC}/KE_{BT} for all throughput values.

Horizontal length scales of modal energies are plotted versus throughput in Fig. 4. Except where noted, length scales in this paper are computed as reciprocals of the first moments (centroids) of wavenumber spectra. A domain-filling eddy would have wavelength $20\pi L_d$ and length scale $10L_d$. The length scale of baroclinic kinetic energy is always near L_d. The barotropic and baroclinic kinetic energy length scales are very nearly equal in the equivalent barotropic regime by virtue of the mode-locking described above. In this limit, the length scales of potential and total energy increase with increasing friction, as they increase with time in freely decaying equivalent barotropic flow (Larichev and McWilliams 1991; Arbic and Flierl 2003). This contrasts with the weakly damped regime, in which the barotropic scale increases with decreasing friction, as it increases with time in freely decaying stratified flow (Rhines 1977). Domain size affects both our least and most viscous experiments. In these the barotropic and potential energy spectra (not shown), respectively, are red out to the largest scales.

Figure 5 plots as a function of throughput the length scales of layer kinetic energies, which can be written in terms of modes:

$$(\nabla\psi_1)^2 = (\nabla\psi_{BT})^2 + \frac{1}{\delta}(\nabla\psi_{BC})^2 + \frac{2}{\sqrt{\delta}}\nabla\psi_{BT}\cdot\nabla\psi_{BC}$$

and

$$(\nabla\psi_2)^2 = (\nabla\psi_{BT})^2 + \delta(\nabla\psi_{BC})^2 - 2\sqrt{\delta}\nabla\psi_{BT}\cdot\nabla\psi_{BC}. \quad (11)$$

When $\delta = 0.2$, the baroclinic mode is weighted more heavily than the barotropic mode in the top layer, while the barotropic mode is weighted more in the bottom layer. Therefore, when damping is weak, the upper-layer length scale remains closer to that of the baroclinic mode, L_d, than does the lower-layer scale, which increases with the barotropic cascade as friction decreases. There is some evidence for a slight increase in length scale with depth in current-meter records (cf. Mercier and Colin de Verdiére 1985, p. 174). Barotropic and baroclinic modes contribute equally to both layer kinetic energies when $\delta = 1$, thus there is less difference between the layer scales.

The ratio of potential to total kinetic energy is plotted versus throughput in Fig. 6a. Potential energy dominates the equivalent barotropic regime, while kinetic energy dominates the barotropic limit. Modal energies in the $\delta = 0.2$ case are plotted in Fig. 6b (the $\delta = 1$ case behaves similarly). The modal energy that changes most rapidly with friction is the one associated with the cascading length scale, that is, potential (barotropic) energy in the strongly (weakly) damped limit. Note that potential en-

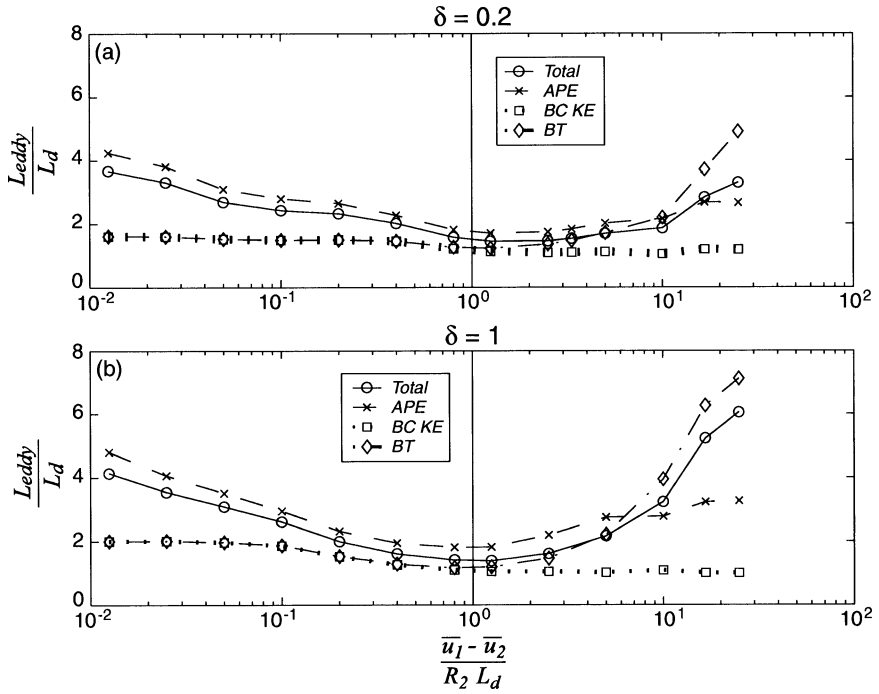

FIG. 4. Horizontal length scales of the different modal energies vs throughput in the f-plane (a) $\delta = 0.2$ and (b) $\delta = 1$ experiments.

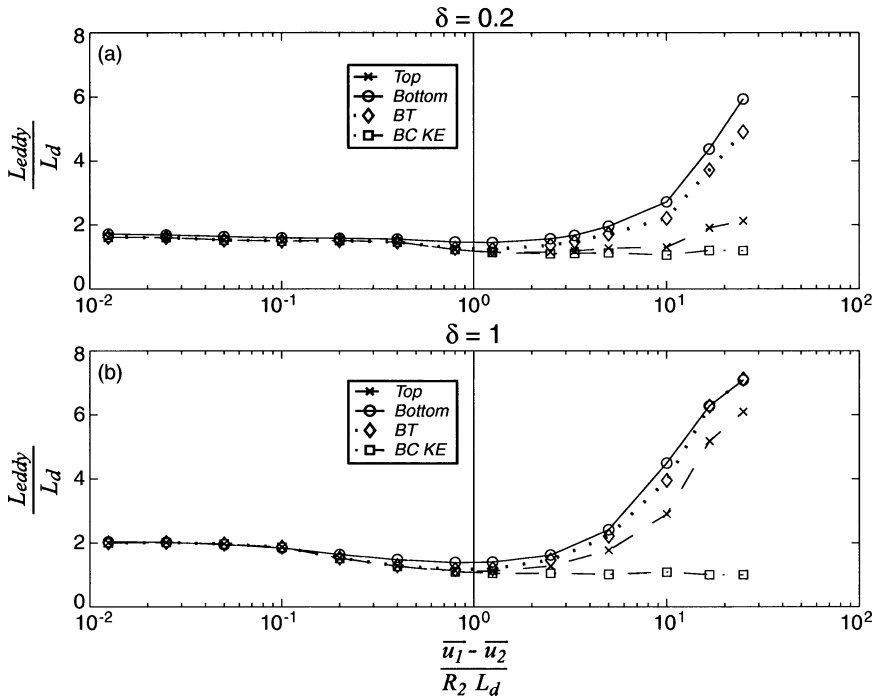

FIG. 5. Horizontal length scales of upper- and lower-layer kinetic energy vs throughput in the f-plane (a) $\delta = 0.2$ and (b) $\delta = 1$ experiments. Length scales of modal kinetic energies are also shown.

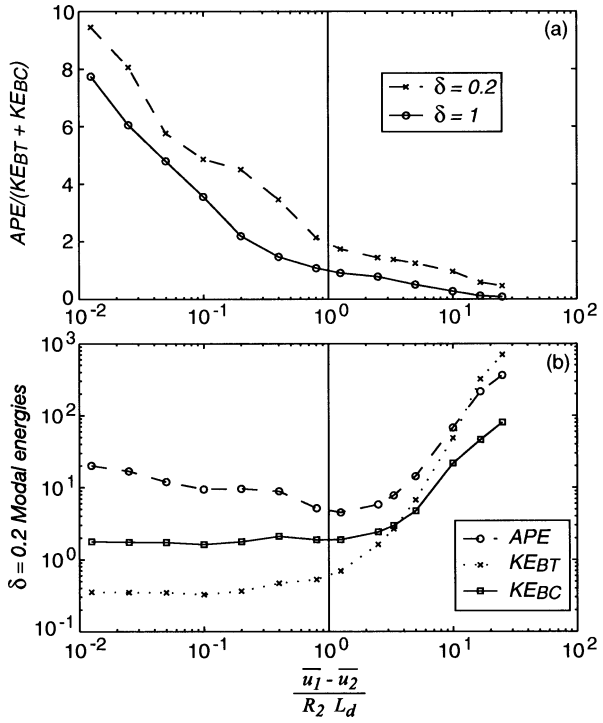

FIG. 6. (a) Ratio of potential to total kinetic energy vs throughput in the f-plane experiments ($\delta = 0.2$ and 1). (b) Modal energies vs throughput in $\delta = 0.2$ f-plane experiments.

ergy is nonmonotonic with friction. Nothing we have found in linear stability analyses points toward the possibility of nonmonotonic behavior. Maximum linear growth rates monotonically decrease with increasing friction, though they are always nonzero (Williams and Robinson 1974; Pedlosky 1983). Thus we believe the nonmonotonic behavior is due to the fact that the moderately damped limit lies between two nonlinear, cascading regimes. Baroclinic kinetic energy increases with decreasing friction in the weakly damped limit. Hua and Haidvogel (1986) demonstrated that bottom friction can act as a source of baroclinic energy. The $\nabla\psi_{\mathrm{BT}} \cdot \nabla\psi_{\mathrm{BC}}$ term in (9) is the only frictional term that could be positive in our two-layer model runs.

Under strong damping, we have seen that kinetic energy length scales are substantially less than those of potential energy. Kinetic energy density concentrates into tight ribbons, wrapped around large regions of diffuse potential energy density (Figs. 7a,b). When throughput is order 1, both potential and kinetic energies have length scales near L_d. The large regions of potential energy density in the strongly damped regime break up into many smaller structures, with weak kinetic energy ribbons wrapped around cores of diffuse potential energy (Figs. 7c,d). When throughput is large, kinetic energy density is diffuse except in the cores of strong coherent vortices (Figs. 7e,f). The changes of potential and kinetic energy density with throughput are discussed in more detail in Arbic and Flierl (2003). The progression from the fronts of the viscous regime to the densely packed weak irregular vortices of the moderately damped regime to the domain-filling two-vortex state of the weakly damped regime is clearly seen in Fig. 8, which displays snapshots of ψ_1 for six throughput values.

d. A scaling for the viscous regime

In Arbic and Flierl (2003) we documented the similarity of the inverse cascades in length scale of potential energy seen in the strongly damped regime and in freely decaying equivalent barotropic flow. We now put forth a scaling that strengthens our claim that increasing friction in the strongly damped regime leads to an equivalent barotropic cascade. Our scaling is in the spirit of those done by Held and Larichev (1996), Spall (2000), and Smith and Vallis (2002), but we will not set the eddy length scale to $\sqrt{U/\beta}$ as these did. Unlike Held and Larichev (1996) and Smith and Vallis (2002) we use layer rather than modal variables. Modal variables are appropriate in the weakly damped limit, in which the layer flows are similar but the modal flows are very different. Layer variables are more appropriate in the strongly damped regime, since upper- and lower-layer flows are very different while the modes are locked together as noted earlier. Following Held and Larichev (1996), we write the rate of energy cascade ϵ_c through the system as U^3/L, but occurring in the upper layer:

$$\epsilon_c \sim \frac{\delta U_1^3}{(1 + \delta)L}. \tag{12}$$

We take the cascading length scale L to be that of APE. From (8), we scale energy production (ϵ_p) and dissipation (ϵ_d) as

$$\epsilon_p \sim \frac{\delta(\overline{u_1} - \overline{u_2})U_1U_2L}{(1 + \delta)^2L_d^2} \quad \text{and} \quad \epsilon_d \sim \frac{R_2U_2^2}{1 + \delta}, \tag{13}$$

where U_2 is the time- and domain-averaged rms lower-layer eddy velocity.

Through rms evaluation of terms in (2), we find that the lower-layer PV balance is $\partial q_2/\partial t \sim R_2\nabla^2\psi_2$. Assuming that the time scale is L/U_1 and that q_2 is dominated by ψ_1, we have

$$\frac{U_1}{L}\frac{\delta U_1 L}{(1 + \delta)L_d^2} \sim \frac{R_2U_2}{L}. \tag{14}$$

Setting ϵ_c, ϵ_p, and ϵ_d equal to each other, and using (14), yields

$$L \sim \frac{(1 + \delta)^{2/3}}{\delta^{1/3}}L_d\left(\frac{\overline{u_1} - \overline{u_2}}{R_2L_d}\right)^{-1/3},$$

$$\mathrm{APE} \sim \frac{\delta\psi_1^2}{2(1 + \delta)^2L_d^2}$$

$$\sim \frac{\delta^{1/3}}{2(1 + \delta)^{2/3}}(\overline{u_1} - \overline{u_2})^2\left(\frac{\overline{u_1} - \overline{u_2}}{R_2L_d}\right)^{-2/3},$$

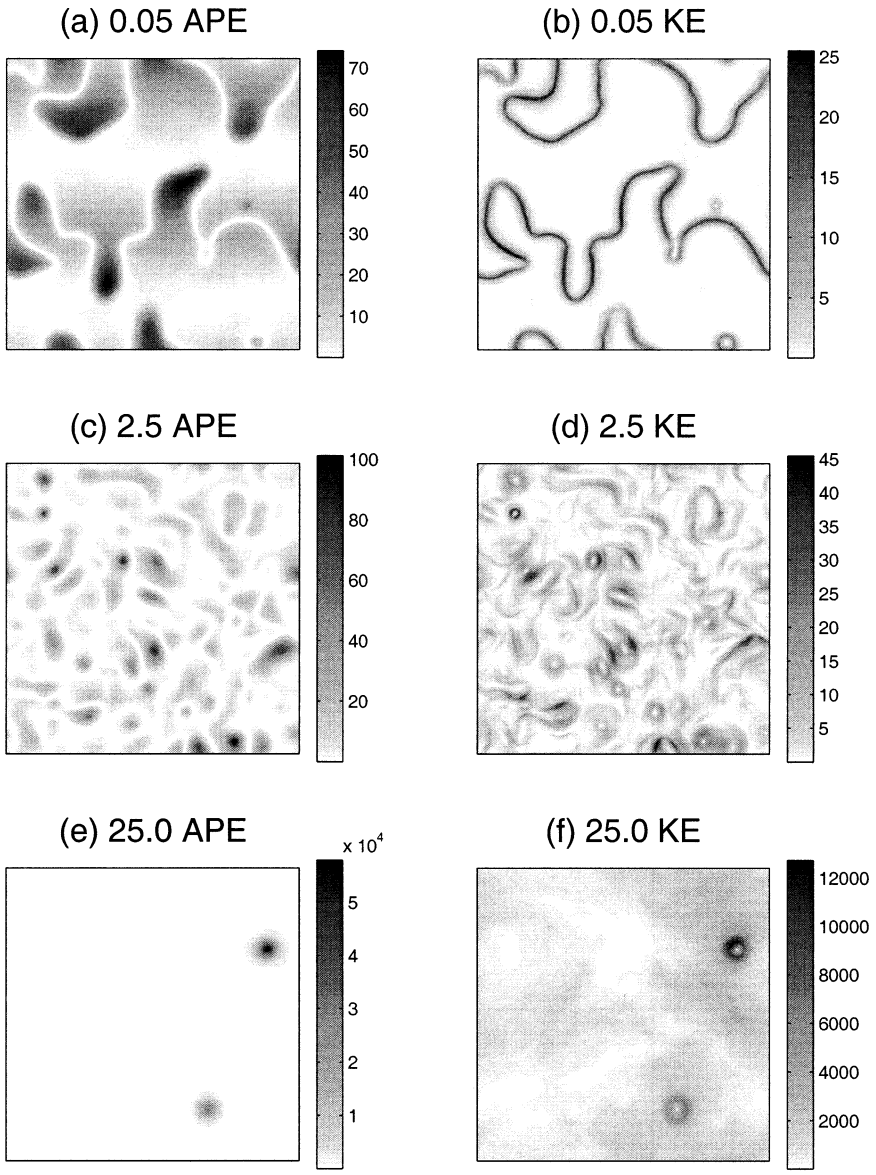

FIG. 7. Potential and kinetic energy densities in snapshots of $\delta = 0.2$ and throughput 0.05, 2.5, and 25.0 f-plane experiments.

$$U_1 \sim (\overline{u_1} - \overline{u_2}),$$

$$U_2 \sim \frac{\delta^{2/3}}{(1+\delta)^{1/3}}(\overline{u_1} - \overline{u_2})\left(\frac{\overline{u_1} - \overline{u_2}}{R_2 L_d}\right)^{2/3},$$

$$\epsilon_p \sim \frac{\delta^{4/3}}{(1+\delta)^{2/3}}\frac{(\overline{u_1} - \overline{u_2})^3}{L_d}\left(\frac{\overline{u_1} - \overline{u_2}}{R_2 L_d}\right)^{1/3}, \quad \text{and}$$

$$\frac{J(\psi_2, q_2)}{\text{Ekman}} \sim \frac{\delta U_1 L}{(1+\delta)L_d^2 R_2} \sim \frac{\delta^{2/3}}{(1+\delta)^{1/3}}\left(\frac{\overline{u_1} - \overline{u_2}}{R_2 L_d}\right)^{2/3}, \tag{15}$$

where ψ_2 was neglected in APE. Figure 9 plots these six quantities, taken from the simulations, versus throughput. Predicted slopes from the scaling are plotted alongside. Dependencies on δ are not borne out for all quantities. The simulations do not match the predicted slopes quantitatively, perhaps due to the domain size effects discussed earlier. However the scaling does give the correct sense of the changes that occur in the strongly damped numerical experiments. Potential energy length scale and potential energy both increase with increasing friction. Upper-layer kinetic energy is roughly independent of friction. The scaling suggests that

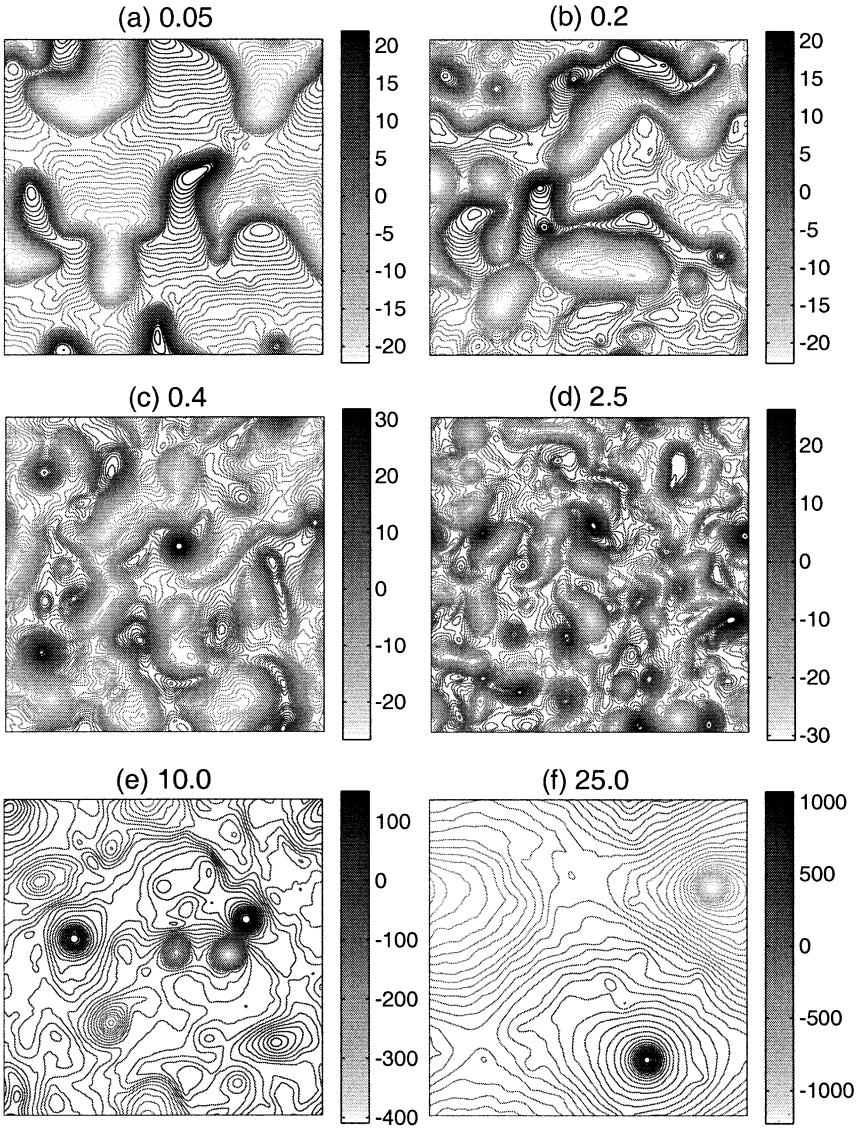

FIG. 8. Snapshots of ψ_1 vs throughput for selected f-plane $\delta = 0.2$ experiments.

upper-layer eddy velocities will be equal to those of the mean flow, while lower-layer velocities will be equal to the mean for order-1 throughput. Scalings are typically off by small factors, and we expect lower-layer velocities to be smaller than upper-layer velocities. In the simulations upper-layer kinetic energy is actually one order of magnitude larger than the mean, while lower-layer kinetic energy is comparable to the mean for order-1 throughput and then decreases as friction increases. Energy production decreases with increasing friction. The ratio of nonlinearity to friction becomes small as friction increases, so that the scaling is self-consistent. All quantities plotted in Fig. 9 are order 1 (or, in some cases, order 1–10) when throughput is 1, as expected. The scaling predicts the ratio of potential to kinetic energy to be much greater than 1 for strong friction, and order 1 in the moderately damped case, in qualitative agreement with Fig. 6a.

As far as we know, our viscous regime scaling is the first to express properties of f-plane turbulence solely in terms of externally imposed quantities. Smith and Vallis (2002) discuss the difficulties of f-plane scalings. The f-plane scaling in Larichev and Held (1995) used eddy lengths taken empirically from their model results. A scaling for weakly damped f-plane turbulence eludes us, as it has thus far eluded others.

e. Comparison of moderately damped regime with observations

The ratio of upper-layer eddy kinetic energy to mean kinetic energy is of order 10 in the strongly damped

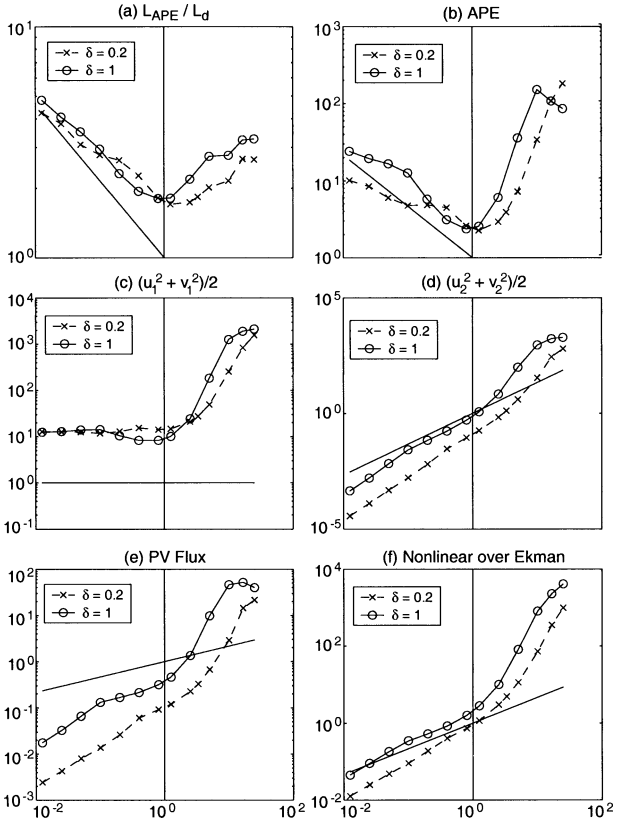

FIG. 9. Test of the scaling developed for the viscous regime for the six quantities in (15). The horizontal axis in all plots is throughput, $(\overline{u_1} - \overline{u_2})/R_2L_d$. The extra straight lines in the plots are predicted slopes from the scaling given in (15). The PV flux ϵ_p in (e) is in units of $(\overline{u_1} - \overline{u_2})^3/L_d$. Although numerical results are plotted for both the strongly and weakly damped limits, the scalings are meant to apply only to the strongly damped limits, that is, the left half of each plot.

regime, order 10–100 in the moderately damped regime, and much higher with weak friction. In the 0.2/2.5 experiment, this ratio is 21, which compares well to observations (cf. Gill et al. 1974; Wunsch 2001).

The upper bound H_2/H_1 on KE_{BC}/KE_{BT} exceeds 1 only when stratification is surface intensified. With weak damping, KE_{BC}/KE_{BT} is much less than H_2/H_1. With moderate damping, KE_{BC}/KE_{BT} is less but not much less than H_2/H_1, which is 5 when $\delta = 0.2$. In the 0.2/2.5 experiment, KE_{BC}/KE_{BT} is 1.5, which compares well to observations (cf. Wunsch 1997 and references therein). The strength and ''bottomness'' of friction, together with surface-intensified stratification, apparently exerts a strong control on eddy baroclinicity. The ratio of upper- to lower-layer squared velocities exceeds 10^5 in our most strongly damped experiments, and approaches 1 when damping is weak. With moderate damping, the ratio is much less than 10^5 but much larger than 1 (of order 10–100). In the 0.2/2.5 experiment, the ratio is 31, which compares well to observations (cf. Mercier and Colin de Verdiére 1985; Müller and Siedler 1992). For equal throughput values, the ratio is significantly higher when $\delta = 0.2$ than when $\delta = 1$. This is because when $\delta = 0.2$, KE_{BC} is weighted more heavily in the upper layer, the ratio KE_{BC}/KE_{BT} is higher, and the layer squared velocity ratio in the baroclinic mode is 25, as compared with a value of 1 when $\delta = 1$.

Extrapolation of our viscous regime scaling to order-1 throughput yields a potential energy length scale near L_d. The length scale of baroclinic kinetic energy is also near L_d, since it is by definition smaller. Therefore by virtue of the relationship $\psi_{BC} \approx \psi_{BT}/\sqrt{\delta}$ in the strongly damped limit, the barotropic length scale must be near L_d. Since modal kinetic energy length scales are near L_d, layer kinetic energy scales will be also. The 0.2/2.5 experiment has an upper-layer scale ($L_{surface}$) of 1.1 L_d, consistent with the correlation between L_d and eddy scales found by Stammer (1997). Let us assume that $\overline{u_1} - \overline{u_2}$ and R_2 are roughly constant in latitude. As L_d decreases by a factor of about 10 from low to high latitudes (Stammer 1997), throughput increases by the same factor. We therefore predict $L_{surface}/L_d$ to increase with latitude. Figure 25 of Stammer (1997) shows this ratio increasing from about 2 in low latitudes to about 3 in high latitudes. In our f-plane simulations, as throughput increases from 2.5 to 25, $L_{surface}/L_d$ increases from 1.1 to 2.1. To be more consistent with Stammer (1997), we could measure upper-layer length scale as the reciprocal of the wavenumber of maximum kinetic energy. Then $L_{surface}/L_d$ changes from 1.4 to 3.3 as throughput increases from 2.5 to 10. Smith and Vallis (2001, 2002) have also pointed out that baroclinic kinetic energy is concentrated near the L_d scale, and is weighted more heavily at the surface when stratification is surface intensified. They argue that this may be related to the correlation of surface eddy length scales with L_d. However, they did not display their model upper-layer length scale, which is the quantity corresponding most closely with what the altimeter sees. Their experiments were in the freely decaying and weakly damped regimes and thus were dominated by the barotropic mode, which is not concentrated near the L_d scale.

The 0.2/2.5 experiment has a potential energy–to–kinetic energy ratio of 1.4. In current-meter data, this ratio is about 5, with higher baroclinic modes typically containing 50%–70% of the potential energy (Wunsch 1999a). Multilayer experiments might therefore be expected to have more realistic ratios of potential to kinetic energy than those in our two-layer experiments.

The appearance of the moderately damped regime also resembles that of observations—compare with MODE Group (1978) and reanalysis maps from the POMME campaign online at http://www.ipsl.jussieu.fr/POMME. Figure 10a displays sea surface height for a portion of the eastern North Atlantic, obtained from the 22 October 1992 snapshot of combined TOPEX/Poseidon–ERS altimeter data (courtesy G. Gebbie, original mapping done by Vinca Rosmorduc at Collecte Localisation Satellites). Figure 10b shows ψ_1 for a quarter-

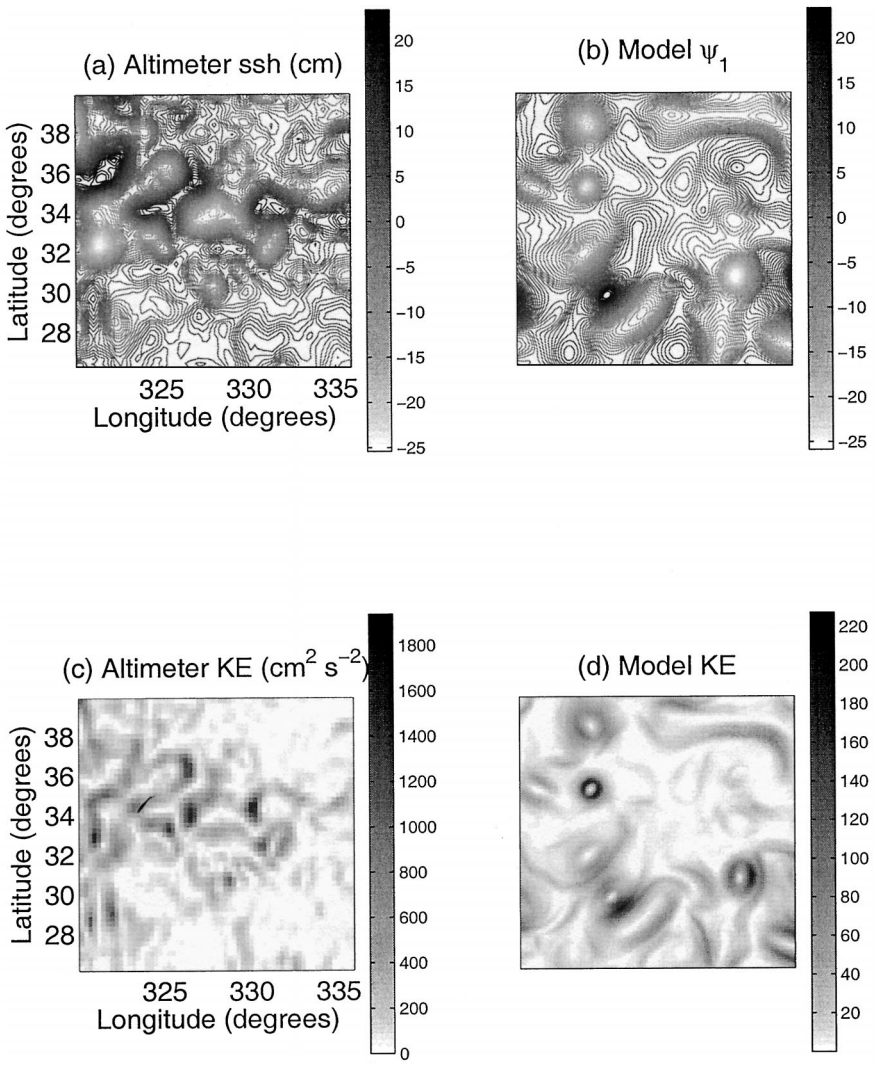

FIG. 10. (a) Eastern North Atlantic sea surface height for the 22 Oct 1992 snapshot of combined TOPEX/Poseidon–ERS altimetry. (b) The ψ_1 for a quarter-domain sized portion of a snapshot of the 0.2/2.5 f-plane experiment. (c) Surface kinetic energy density for the altimeter snapshot. (d) Upper-layer kinetic energy density of the 0.2/2.5 f-plane experiment.

domain portion of a snapshot of the 0.2/2.5 experiment (the portion has nearly the same spatial dimensions as the altimetry snapshot). Figure 10c displays kinetic energy density for the altimetry snapshot. We calculated velocities by center differencing the sea surface height field and using the geostrophic relations. Figure 10d displays the kinetic energy density of the quarter-domain 0.2/2.5 snapshot. Weak kinetic energy tendrils similar to those in the model snapshot are arguably present in the altimetry snapshot. Certainly, the kinetic energy densities and streamfunctions in the small and large throughput cases (Figs. 7 and 8) do not resemble those in observations as closely as do those in the moderately damped regime.

We conclude section 4e with a comparison with observed midocean eddy heat fluxes. A primary motivation for studying eddies has been development of eddy heat flux parameterizations (cf. Gent and McWilliams 1990; Hogg 1993; Larichev and Held 1995; Wardle and Marshall 2000; Smith and Vallis 2002). Estimates of eddy fluxes on global or near-global scales have been made from current meters (Wunsch 1999b) and from satellite altimeters (Stammer 1998; adapted from methods developed in Holloway 1986 and Keffer and Holloway 1988). Both the Wunsch and Stammer estimates suggest that eddy heat fluxes are important, relative to the total meridional oceanic heat flux, in western boundary currents and in the southern ocean. In the ocean interior, however, eddy fluxes may be as little as 1% of the total. Since our model transports heat only through eddies, we cannot normalize eddy fluxes against a total transport. Instead we convert eddy PV fluxes in our δ

$= 0.2$ experiments into heat fluxes appropriate for a QG continuously stratified ocean, with density perturbations

$$\rho' = -\frac{\rho_0 f_0}{g}\frac{\partial \psi}{\partial z} \tag{16}$$

(Pedlosky 1987). We assume that the first baroclinic mode $\psi_{\mathrm{BC}}(x, y, t)$ dominates ρ' and write $\psi = \psi_{\mathrm{BT}}(x, y, t) + \psi_{\mathrm{BC}}(x, y, t)F(z)$. Therefore,

$$\rho' = -\frac{\rho_0 f_0 \psi_{\mathrm{BC}}(x, y, t)}{g}\frac{dF}{dz}. \tag{17}$$

Assuming a linear equation of state, we write ρ' in terms of potential temperature (salinity) fluctuations θ' (S') and thermal expansion (haline contraction) coefficients α (β):

$$\rho' = \rho_0(-\alpha\theta' + \beta S'). \tag{18}$$

By further assuming a linear θ–S relationship, we have

$$\rho' = \rho_0\left(\beta\frac{\partial S}{\partial \theta} - \alpha\right)\theta'. \tag{19}$$

We use (17) and (19) to relate ψ_{BC} to θ':

$$\psi_{\mathrm{BC}} = -\frac{g\left(\beta\dfrac{\partial S}{\partial \theta} - \alpha\right)}{f_0\dfrac{dF}{dz}}\theta'. \tag{20}$$

By equating ψ_{BC} in the continuous and two-layer cases, we rewrite the model upper-layer PV flux

$$\overline{v_1 q_1} = \frac{\overline{v_1(\psi_2 - \psi_1)}}{(1+\delta)L_d^2} = -\frac{\overline{v_1\psi_{\mathrm{BC}}}}{\sqrt{\delta}L_d^2} = \frac{g\left(\beta\dfrac{\partial S}{\partial \theta} - \alpha\right)}{\sqrt{\delta} f_0 L_d^2 \dfrac{dF}{dz}}\overline{v_1\theta'}. \tag{21}$$

(In homogeneous models, momentum flux does not contribute to PV flux.) The eddy heat flux integrated over the thermocline will be approximately

$$\text{Heat flux} \approx \rho_0 c_p L_{\mathrm{thermocline}}\overline{v_1\theta'}$$

$$\approx \frac{\sqrt{\delta}\rho_0 c_p L_{\mathrm{thermocline}} f_0 L_d^2 \dfrac{dF}{dz}}{g\left(\beta\dfrac{\partial S}{\partial \theta} - \alpha\right)}\overline{v_1 q_1}, \tag{22}$$

where c_p is heat capacity and $L_{\mathrm{thermocline}}$ is thermocline depth. We use hydrographic station 169 of the 1981 Atlantis 109 cruise (latitude 24.5°N, longitude 28.6°W; Roemmich and Wunsch 1985) as a representative vertical profile in the eastern North Atlantic subtropical gyre. We calculate $F(z)$ for the first baroclinic mode in the usual manner (cf. Richman 1976). The maximum value of dF/dz, and thus ρ', in the lower thermocline occurs at 800 m. The θ–S relationship is nearly linear over 600–1000 m, and we estimate $\partial S/\partial\theta$ with a least squares fit over this range. We evaluate (dF/dz), β, and α at 800 m and take $\rho_0 = 1030$ kg m^{-3}, $c_p = 4000$ J kg^{-1} K^{-1}, $L_{\mathrm{thermocline}} = 1000$ m, $f_0 = 6.0 \times 10^{-5}$ s^{-1}, and $g = 9.8$ m s^{-2}. Heat flux is plotted against throughput in Fig. 11. An extra horizontal line is drawn at 5×10^6 W m^{-1}, a typical value for the top 1000 m in subtropical gyre interiors (Stammer 1998; Wunsch 1999b). Results from our throughput = 3.33 and throughput = 5 experiments match this nominal value most closely. Fluxes in the throughput = 25 experiment are 41 times as large, and fluxes in the throughput = 0.0125 experiment are a factor of 214 smaller. Because of the many shortcomings of our model, we believe these results are merely suggestive. But the suggestion is that eddy fluxes, like other eddy properties, match observations best when throughput is of order 1. Under weak damping, model eddies have larger horizontal scales than do observed eddies. Large eddies create large PV anomalies, and therefore, large eddy fluxes. Large generation is needed to balance bottom dissipation, which is large because the eddies are more energetic and more barotropic than in observations. The weakly damped regime is physically consistent, but is not consistent with observations. Under strong damping, dissipation and production are weaker than in observations. The moderately damped regime has realistic bottom layer velocities, hence realistic dissipation rates. Thus the generation balancing this dissipation will be realistic.

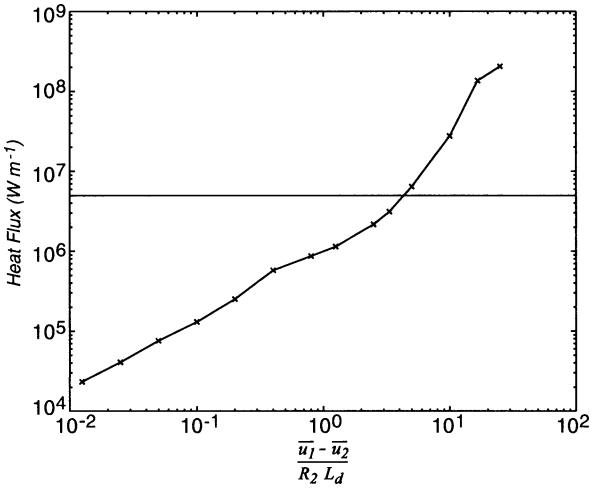

FIG. 11. Upper-layer potential vorticity fluxes vs throughput in the $\delta = 0.2$ f-plane experiments, converted to dimensional estimates of eddy heat fluxes in the top 1000 m of a continuously stratified ocean. Horizontal line indicates value of 5×10^6 W m^{-1}, a typical eddy heat flux in midlatitude midocean gyres.

5. Beta-plane experiments

The governing β-plane equations are

$$\frac{\partial q_1}{\partial t} + \overline{u_1}\frac{\partial q_1}{\partial x} + \overline{v_1}\frac{\partial q_1}{\partial y} - \frac{\partial \overline{q_1}}{\partial x}\frac{\partial \psi_1}{\partial y} + \frac{\partial \overline{q_1}}{\partial y}\frac{\partial \psi_1}{\partial x} + J(\psi_1, q_1) = \text{ssd} \quad \text{and} \tag{23}$$

$$\frac{\partial q_2}{\partial t} + \overline{u_2}\frac{\partial q_2}{\partial x} + \overline{v_2}\frac{\partial q_2}{\partial y} - \frac{\partial \overline{q_2}}{\partial x}\frac{\partial \psi_2}{\partial y} + \frac{\partial \overline{q_2}}{\partial y}\frac{\partial \psi_2}{\partial x} + J(\psi_2, q_2) = -R_2\nabla^2\psi_2 + \text{ssd}, \tag{24}$$

with mean PV gradients

$$\frac{\partial \overline{q_1}}{\partial x} = \frac{(\overline{v_2} - \overline{v_1})}{(1+\delta)L_d^2}, \qquad \frac{\partial \overline{q_2}}{\partial x} = \frac{\delta(\overline{v_1} - \overline{v_2})}{(1+\delta)L_d^2},$$
$$\frac{\partial \overline{q_1}}{\partial y} = \beta + \frac{(\overline{u_1} - \overline{u_2})}{(1+\delta)L_d^2}, \quad \text{and}$$
$$\frac{\partial \overline{q_2}}{\partial y} = \beta + \frac{\delta(\overline{u_2} - \overline{u_1})}{(1+\delta)L_d^2}. \tag{25}$$

Zonal mean flows are stabilized by large β, which prevents meridional PV gradients from changing sign between layers (Charney and Stern 1962), although small growth rates can still arise from the destabilizing effects of friction (Holopainen 1961). Nonzonal mean flows are more unstable because they create zonal gradients that change sign regardless of β. Since zonal gradients are independent of β, we expect to see similarities between beta-plane turbulence driven by nonzonal mean flows and f-plane turbulence. All simulations in this section have $\delta = 0.2$ and $\sqrt{(\overline{u_1} - \overline{u_2})^2 + (\overline{v_1} - \overline{v_2})^2} = 1$ cm s^{-1}. We define $P_S = \beta$/upper-layer shear gradient $= \beta(1+\delta)L_d^2/\sqrt{(\overline{u_1} - \overline{u_2})^2 + (\overline{v_1} - \overline{v_2})^2}$. Energies are normalized by $[(\overline{u_1} - \overline{u_2})^2 + (\overline{v_1} - \overline{v_2})^2]/2$, and throughput is equal to $\sqrt{(\overline{u_1} - \overline{u_2})^2 + (\overline{v_1} - \overline{v_2})^2}/R_2L_d$. We satisfy $J(\overline{\psi}, \overline{q}) = 0$ with a procedure described in Arbic and Flierl (2004).

Given our chosen parameters and a typical midlatitude value of $\beta = 2 \times 10^{-11}$ m^{-1} s^{-1}, $P_S = 6$. In this case energetic eddies are produced only when the mean flow is nonzonal (Arbic and Flierl 2004). As discussed earlier, the two-layer model probably underestimates shear-induced mean PV gradients. As discussed in Arbic and Flierl (2004), PV maps (Keffer 1985) suggest that planetary and shear-induced gradients are comparable. Thus, in this section we perform experiments with β values that are artifically small, to compensate for the underestimated shear. Figure 12 plots modal length scales versus throughput for four sets of beta-plane experiments, distinguished from each other by their P_S values (0.093 75 vs 0.1875) and mean shear directions (eastward vs 30° south of east). In the strongly damped regime, eddy energy (not shown) does not increase with increasing friction as on the f plane. However, the increase in potential energy length scale with increasing friction survives the presence of at least these small β values. In the weakly damped limit, the barotropic length scale increases with decreasing friction, although the increase is slight in the zonal $P_S = 0.1875$ experiments.

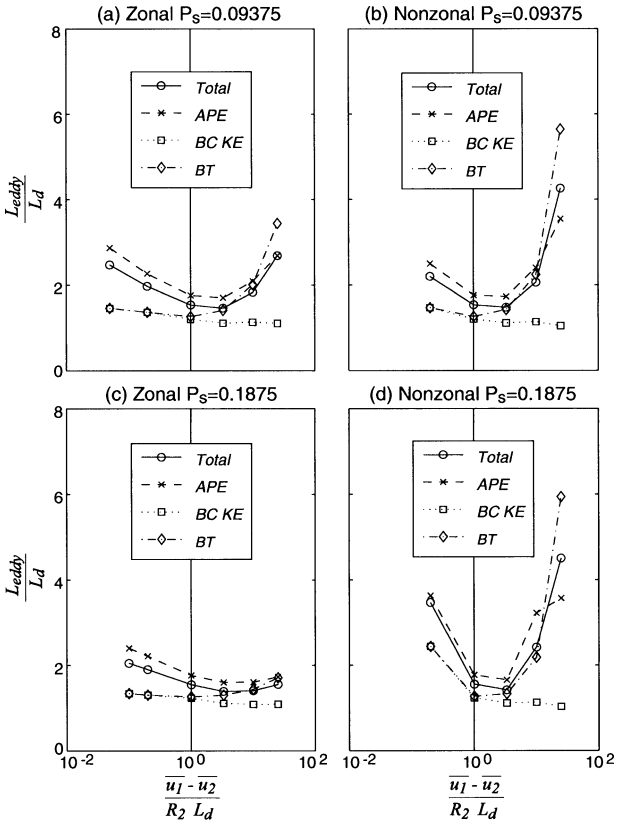

FIG. 12. Horizontal length scales of the different modal energies vs throughput for $\delta = 0.2$ beta-plane simulations with $P_S = 0.093\,75$ and $P_S = 0.1875$. Zonal simulations have eastward mean flows and nonzonal simulations have a shear flow 30° south of east.

Figures 13a and 13b plot upper-layer eddy kinetic energy versus throughput for the same four sets of simulations; f-plane results are included alongside for comparison. Although the entire range of throughput values is displayed, the following discussion pertains only to the weakly damped limit. In agreement with Panetta (1993) and Smith and Vallis (2002), energy exhibits little sensitivity to friction in beta-plane turbulence driven by eastward mean flows. The barotropic kinetic energies (not shown) in the weakly damped limit of the eastward $P_S = 0.093\,75$ and 0.1875 experiments have a 1.15 and 0.30 power-law dependence on throughput, respectively, as determined by a least squares fit over throughput values greater than 1. Smith and Vallis (2002) found a value of 1 in their eastward experiments. As anticipated, the nonzonal beta-plane case resembles the f plane. Energy has great sensitivity to friction, such that realistic ratios (order 10–100) of upper-layer eddy to mean kinetic energy arise only when throughput is order 1. The barotropic kinetic energies in the weakly damped limit of the nonzonal $P_S = 0.093\,75$ and 0.1875

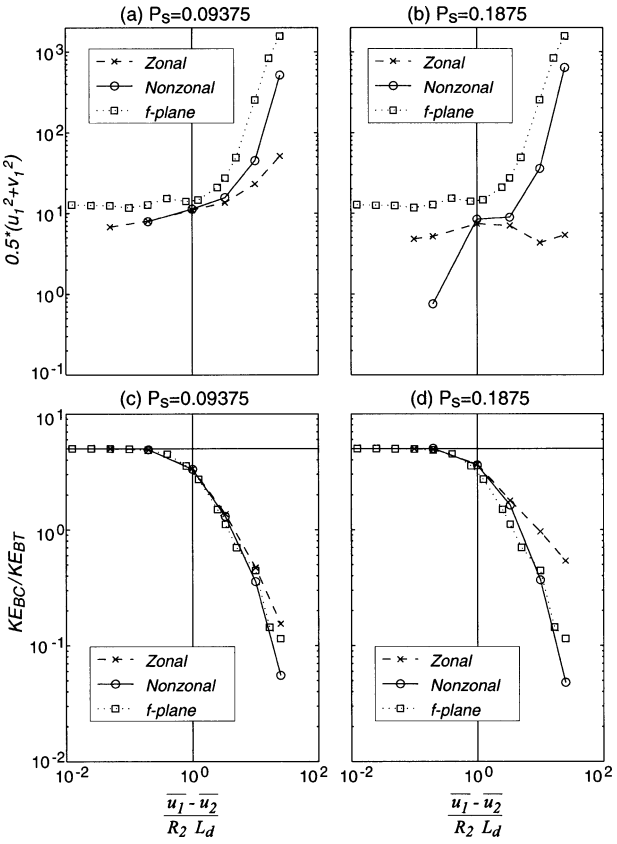

FIG. 13. Upper-layer kinetic energy vs throughput for $\delta = 0.2$ beta-plane simulations with (a) $P_S = 0.09375$ and (b) 0.1875. Beta-plane experiments with both zonal and nonzonal mean flows are shown. For comparison, f-plane solutions are plotted alongside in each panel. Zonal simulations have eastward mean flows, and nonzonal simulations have a shear flow 30° south of east. KE_{BC}/KE_{BT} is plotted vs throughput for the same sets of experiments in (c) and (d).

experiments have a steeper 1.97 and 2.19 dependence on throughput, respectively, closer to the 2.47 dependence found on the f plane. Differences between eastward and nonzonal beta-plane experiments are more marked for the larger P_S value. Sensitivity to friction is also large in $P_S = 6$ experiments with mean flows 30° south of west (Arbic and Flierl 2004). In the lack of a sensitivity of eddy energy to friction, beta-plane turbulence forced by eastward mean flows is apparently a special case. In both zonal and nonzonal beta-plane simulations, the baroclinic to barotropic kinetic energy ratio (Figs. 13c,d) matches observations best when throughput is order 1; again, the nonzonal results resemble the f-plane results more closely.

6. Summary and discussion

Midocean eddies have kinetic energies larger than that of the mean flow, while retaining substantial kinetic energy in the first baroclinic mode and in horizontal scales near L_d. In this paper we have asked whether horizontally homogeneous, baroclinically unstable 2-layer QG turbulence dissipated by bottom friction can meet all of these criteria. We have varied friction over a much greater range than any previous QG turbulence study, and are the first to explore the strongly damped limit. Eddy properties in the strongly and weakly damped (small and large throughput) limits are relatively easy to understand, and are used to explain those in the moderately damped regime (order-1 throughput), which compares well to observations. Our estimate of throughput is highly uncertain, but it seems possible that it is order 1 over large parts of the midlatitude midocean.

The strongly damped limit is equivalent barotropic (bottom layer flow is nearly zero) and is characterized by an increase in the length scale of potential energy with increasing friction. A scaling based on this cascade was developed. Extrapolating it to order-1 friction suggests that in that case upper-layer eddy velocities will be somewhat larger than the mean, eddy horizontal length scales will be near L_d, and KE_{BC}/KE_{BT} will be near its upper bound H_2/H_1, which can exceed 1 only if stratification is surface-intensified. The 0.2/2.5 case has ratios of surface eddy to mean kinetic energy, KE_{BC}/KE_{BT}, upper- to lower-layer squared velocities, and $L_{surface}/L_d$ that compare well to observations. Our arguments predict an increase in $L_{surface}/L_d$ as L_d decreases with increasing latitude, and this behavior is also seen in the data. The moderately damped limit consists of densely packed irregular weak vortices surrounded by weak ribbons of kinetic energy, and resembles the appearance of midocean eddies more closely than do the strongly and weakly damped limits. Last, eddy heat fluxes also apparently match observations best in the moderately damped regime. All of this answers the central question of the paper in the affirmative and represents a point of departure from previous flat-bottom QG turbulence studies. These work in the limit of weak drag and undergo the cascade to the barotropic mode and horizontal scales larger than L_d. Our conclusion that horizontal eddy scales are sensitive to friction agrees with that of Riviere et al. (2004), although there are many differences between the two studies. The mean flow in Riviere et al. (2004) was horizontally inhomogeneous, and they utilized primitive equation as well as QG simulations. They studied only the weakly damped regime and varied friction only by a factor of 8.

Consistent with previous studies we find that eddy energy is fairly insensitive to friction in the weakly damped limit of horizontally homogeneous beta-plane turbulence forced by eastward mean flows. However, it is not clear that weak eastward mean flows could produce energetic eddies in the presence of β. Weak nonzonal flows are able to do so. As anticipated by a heuristic argument, beta-plane turbulence driven by nonzonal mean flows resembles f-plane turbulence in that eddy energy is highly sensitive to friction. Thus attaining realistic eddy energies again requires moderate damping. Furthermore, in both eastward and nonzonal beta-plane simulations, realistic values of other quantities such as KE_{BC}/KE_{BT} occur only with order-1 throughput.

We hope to build upon this work by performing multilayer simulations with a range of frictions comparable to that explored here in the two-layer case. The barotropic and first baroclinic modes contain the bulk of the eddy kinetic energy, and neither has much vertical structure beneath the thermocline. Thus the two-layer model probably captures most of the frictional dynamics. Nonetheless, motions in higher baroclinic modes are significant. Current-meter data indicate that in many locations the second baroclinic mode contains 10% as much kinetic energy as the barotropic mode [conclusion based on an extension of Table 1 in Wunsch (1997), provided to us by C. Wunsch]. In midlatitude LADCP data, this ratio can be even higher (S. Chen and E. Firing 2002, personal communication).

Another natural extension of our work would be to explore baroclinically unstable QG turbulence with a wide range of frictions in the presence of rough topography. Apart from its probable effect on dissipation, topography alters PV contours and arrests the cascade to barotropic large-scale flow in freely decaying turbulence (cf. Bretherton and Haidvogel 1976; Rhines 1977; LaCasce and Brink 2000) and in turbulence driven by fluctuating winds (Treguier and Hua 1988). LaCasce (1996) and LaCasce and Brink (2000) suggest that bottom topography and bottom Ekman friction have similar effects on eddies. Thus R_2 and throughput may act as proxies for eddy interactions with topography. Over both smooth and rough regions, LADCP data indicate that eddies are surface trapped. (S. Chen and E. Firing 2002, personal communication). Simulations in inhomogeneous domains may help to determine whether vertical structure developed over rough topography is retained in smooth regions.

Acknowledgments. BKA is profoundly grateful to numerous individuals, listed in the acknowledgements of Arbic (2000), for helping him in various ways to complete his Ph.D. thesis. As that work was further developed into this paper, BKA had helpful discussions with more people, including Baylor Fox-Kemper, Joe LaCasce, Jonas Nycander, Lew Rothstein, Tom Rossby, Dale Haidvogel, Steve Griffies, Shafer Smith, Alain Colin de Verdiére, and Andy Majda. Jim McWilliams was particularly helpful. David Nolan, Guillaume Lapeyre, and the anonymous reviewers greatly improved this manuscript with their comments. Cathy Raphael and Jeff Varanyak helped with the figures. Many people at MIT, WHOI, and GFDL allowed BKA to use their computers. While this research was undertaken, BKA was funded by an Office of Naval Research/National Defense Science and Engineering Graduate Fellowship, Office of Naval Research Grant N00014-95-1-0824, and National Science Foundation Grant OCE-9617848. GRF was also supported by the National Science Foundation grant. This paper was written while BKA was supported by the GFDL/Princeton University Visiting Scientist Program.

REFERENCES

Arbic, B. K., 2000: Generation of mid-ocean eddies: The local baroclinic instability hypothesis. Ph.D. dissertation, Massachusetts Institute of Technology–Woods Hole Oceanographic Institution Joint Program, 290 pp.

——, and G. R. Flierl, 2003: Coherent vortices and kinetic energy ribbons in asymptotic, quasi two-dimensional *f*-plane turbulence. *Phys. Fluids,* **15,** 2177–2189.

——, and ——, 2004: Effects of mean flow direction on energy, isotropy, and coherence of baroclinically unstable beta-plane geostrophic turbulence. *J. Phys. Oceanogr.,* **34,** 77–93.

——, S. T. Garner, R. W. Hallberg, and H. L. Simmons, 2004: The accuracy of surface elevations in forward global barotropic and baroclinic tide models. *Deep-Sea Res.,* in press.

Batchelor, G. K., 1953: *The Theory of Homogeneous Turbulence.* Cambridge University Press, 121 pp.

Bretherton, F. B., and D. B. Haidvogel, 1976: Two-dimensional turbulence over topography. *J. Fluid Mech.,* **78,** 129–154.

Charney, J. G., 1947: The dynamics of long waves in a baroclinic westerly current. *J. Meteor.,* **4,** 135–163.

——, 1971: Geostrophic turbulence. *J. Atmos. Sci.,* **28,** 1087–1095.

——, and M. E. Stern, 1962: On the stability of internal baroclinic jets in a rotating atmosphere. *J. Atmos. Sci.,* **19,** 159–172.

——, and G. R. Flierl, 1981: Oceanic analogues of large-scale atmospheric motions. *Evolution of Physical Oceanography,* B. A. Warren and C. Wunsch, Eds., MIT Press, 504–548.

Cheney, R. E., and P. L. Richardson, 1976: Observed decay of a cyclonic Gulf Stream ring. *Deep-Sea Res.,* **23,** 143–155.

Chester, D., P. Malanotte-Rizzoli, J. Lynch, and C. Wunsch, 1994: The eddy radiation field of the Gulf Stream as measured by ocean acoustic tomography. *Geophys. Res. Lett.,* **21,** 181–184.

Colin de Verdiére, A., H. Mercier, and M. Arhan, 1989: Mesoscale variability transition from the western to the eastern Atlantic along 48°N. *J. Phys. Oceanogr.,* **19,** 1149–1170.

Eady, E. T., 1949: Long waves and cyclone waves. *Tellus,* **1,** 33–52.

Egbert, G. D., and R. D. Ray, 2001: Estimates of M_2 tidal energy dissipation from TOPEX/Poseidon altimeter data. *J. Geophys. Res.,* **106,** 22 475–22 502.

Fjortoft, R., 1953: On the changes in the spectral distributions of kinetic energy for two-dimensional non-divergent flow. *Tellus,* **5,** 225–230.

Flierl, G. R., 1978: Models of vertical structure and the calibration of two-layer models. *Dyn. Atmos. Oceans,* **2,** 341–381.

——, and V. M. Kamenkovich, 1975: Gulf Stream meandering and Gulf Stream ring eddy production mechanisms. *Dynamics and the Analysis of MODE-I,* A. R. Robinson, Ed., MIT Press, 115–118.

Frankignoul, C., and P. Müller, 1979: Quasi-geostrophic response of an infinite β-plane ocean to stochastic forcing by the atmosphere. *J. Phys. Oceanogr.,* **9,** 104–127.

Fu, L.-L., and G. R. Flierl, 1980: Nonlinear energy and enstrophy transfers in a realistically stratified ocean. *Dyn. Atmos. Oceans,* **4,** 219–246.

Gent, P. R., and J. C. McWilliams, 1990: Isopycnal mixing in ocean circulation models. *J. Phys. Oceanogr.,* **20,** 150–155.

Gill, A. E., J. S. A. Green, and A. J. Simmons, 1974: Energy partition in the large-scale ocean circulation and the production of mid-ocean eddies. *Deep-Sea Res.,* **21,** 499–528.

Gille, S. T., M. M. Yale, and D. T. Sandwell, 2000: Global correlation of mesoscale ocean variability with seafloor roughness from satellite altimetry. *Geophys. Res. Lett.,* **27,** 1251–1254.

Haidvogel, D. B., and I. M. Held, 1980: Homogeneous quasigeostrophic turbulence driven by a uniform temperature gradient. *J. Atmos. Sci.,* **37,** 2644–2660.

Held, I. M., and V. D. Larichev, 1996: A scaling theory for horizontally homogeneous, baroclinically unstable flow on a beta plane. *J. Atmos. Sci.,* **53,** 946–952.

Hirose, N., I. Fukimori, V. Zlotnicki, and R. M. Ponte, 2001: Modeling the high-frequency barotropic response of the ocean to atmospheric disturbances: Sensitivity to forcing, topography, and friction. *J. Geophys. Res.,* **106,** 30 987–30 995.

Hogg, N. G., 1985: Evidence for baroclinic instability in the Gulf Stream recirculation. *Progress in Oceanography*, Vol. 14, Persamon, 209–229.
——, 1988: Stochastic wave radiation by the Gulf Stream. *J. Phys. Oceanogr.*, **18,** 1687–1701.
——, 1993: Toward parameterization of the eddy field near the Gulf Stream. *Deep-Sea Res.*, **40,** 2359–2376.
Holloway, G., 1986: Estimation of oceanic eddy transports from satellite altimetry. *Nature*, **323,** 243–244.
Holopainen, E. O., 1961: On the effect of friction in baroclinic waves. *Tellus*, **13,** 363–367.
Hua, B. L., and D. B. Haidvogel, 1986: Numerical simulations of the vertical structure of quasi-geostrophic turbulence. *J. Atmos. Sci.*, **43,** 2923–2936.
Jayne, S. R., and L. C. St. Laurent, 2001: Parameterizing tidal dissipation over rough topography. *Geophys. Res. Lett.*, **28,** 811–814.
Kamenkovich, I. V., and J. Pedlosky, 1996: Radiating instability of nonzonal ocean currents. *J. Phys. Oceanogr.*, **26,** 622–643.
Keffer, T., 1985: The ventilation of the world's oceans: Maps of the potential vorticity field. *J. Phys. Oceanogr.*, **15,** 509–523.
——, and G. Holloway, 1988: Estimating southern ocean eddy flux of heat and salt from satellite altimetry. *Nature*, **332,** 624–626.
LaCasce, J. H., 1996: Baroclinic vortices over a sloping bottom. Ph.D. dissertation, Massachusetts Institute of Technology–Woods Hole Oceanographic Institution Joint Program, 220 pp.
——, and K. H. Brink, 2000: Geostrophic turbulence over a slope. *J. Phys. Oceanogr.*, **30,** 1305–1324.
Lapeyre, G., and I. M. Held, 2003: Diffusivity, kinetic energy dissipation, and closure theories for the poleward eddy heat flux. *J. Atmos. Sci.*, **60,** 2907–2916.
Large, W. G., W. R. Holland, and J. C. Evans, 1991: Quasi-geostrophic response to real wind forcing: The effects of temporal smoothing. *J. Phys. Oceanogr.*, **21,** 998–1017.
Larichev, V. D., and J. C. McWilliams, 1991: Weakly decaying turbulence in an equivalent-barotropic fluid. *Phys. Fluids*, **A3,** 938–950.
——, and I. M. Held, 1995: Eddy amplitudes and fluxes in a homogeneous model of fully developed baroclinic instability. *J. Phys. Oceanogr.*, **25,** 2285–2297.
Maul, G. A., P. W. deWitt, A. Yanaway, and S. R. Baig, 1978: Geostationary satellite observations of Gulf Stream meanders: Infrared measurements and time series analysis. *J. Geophys. Res.*, **83,** 6123–6135.
Mercier, H., and A. Colin de Verdiére, 1985: Space and time scales of mesoscale motions in the eastern North Atlantic. *J. Phys. Oceanogr.*, **15,** 171–183.
MODE Group, 1978: The Mid-Ocean Dynamics Experiment. *Deep-Sea Res.*, **25,** 859–910.
Müller, P., and C. Frankignoul, 1981: Direct atmospheric forcing of geostrophic eddies. *J. Phys. Oceanogr.*, **11,** 287–308.
Müller, T. J., and G. Siedler, 1992: Multi-year current time series in the eastern North Atlantic Ocean. *J. Mar. Res.*, **50,** 63–98.
Munk, W., 1997: Once Again: Once again—Tidal friction. *Progress in Oceanography*, Vol. 40, Pergamon, 7–35.
Panetta, R. L., 1993: Zonal jets in wide baroclinically unstable regions: Persistence and scale selection. *J. Atmos. Sci.*, **50,** 2073–2106.
Pedlosky, J., 1983: The growth and decay of finite-amplitude baroclinic waves. *J. Atmos. Sci.*, **40,** 1863–1876.
——, 1987: *Geophysical Fluid Dynamics*. 2d ed. Springer-Verlag, 710 pp.
Polzin, K. L., J. M. Toole, J. R. Ledwell, and R. W. Schmitt, 1997: Spatial variability of turbulent mixing in the abyssal ocean. *Science*, **276,** 93–96.
Rhines, P. B., 1975: Waves and turbulence on a beta plane. *J. Fluid Mech.*, **69,** 417–443.
——, 1977: The dynamics of unsteady currents. *The Sea*, E. D. Goldberg et al., Eds., Marine Modeling, Vol. 6, John Wiley and Sons, 189–318.
Richardson, P. L., 1983: Gulf Stream rings. *Eddies in Marine Science*, A. R. Robinson, Ed., Springer, 19–45.
Richman, J. G., 1976: Kinematics and energetics of the mesoscale mid-ocean circulation: MODE. Ph.D. dissertation, Massachusetts Institute of Technology–Woods Hole Oceanographic Institution Joint Program, 205 pp.
Riviere, P., and P. L. Klein, 1997: Effects of an asymmetric friction on the nonlinear equilibration of a baroclinic system. *J. Atmos. Sci.*, **54,** 1610–1627.
——, A. M. Treguier, and P. Klein, 2004: Effects of bottom friction on nonlinear equilibration of an oceanic baroclinic jet. *J. Phys. Oceanogr.*, **34,** 416–432.
Robinson, A. R., and J. C. McWilliams, 1974: The baroclinic instability of the open ocean. *J. Phys. Oceanogr.*, **4,** 281–294.
Roemmich, D., and C. Wunsch, 1985: Two transatlantic sections: Meridional circulation and heat flux in the subtropical North Atlantic Ocean. *Deep-Sea Res.*, **32,** 619–664.
Salmon, R., 1978: Two-layer quasi-geostrophic turbulence in a simple special case. *Geophys. Astrophys. Fluid Dyn.*, **10,** 25–52.
——, 1980: Baroclinic instability and geostrophic turbulence. *Geophys. Astrophys. Fluid Dyn.*, **15,** 167–211.
Schmitz, W. J., 1996a: On the World Ocean circulation. Vol. I, Some global features/North Atlantic circulation. Woods Hole Oceanographic Institution Tech. Rep. WHOI-96-03, 140 pp.
——, 1996b: On the World Ocean circulation. Vol. II, The Pacific and Indian Oceans/A global update. Woods Hole Oceanographic Institution Tech. Rep. WHOI-96-08, 237 pp.
Smith, K. S., and G. K. Vallis, 2001: The scales and equilibration of midocean eddies: Freely evolving flow. *J. Phys. Oceanogr.*, **31,** 554–571.
——, and ——, 2002: The scales and equilibration of midocean eddies: Forced–dissipative flow. *J. Phys. Oceanogr.*, **32,** 1699–1720.
——, G. Boccaletti, C. C. Henning, I. N. Marinov, C. Y. Tam, I. M. Held, and G. K. Vallis, 2002: Turbulent diffusion in the geostrophic inverse cascade. *J. Fluid Mech.*, **469,** 13–48.
Spall, M. A., 2000: Generation of strong mesoscale eddies by weak ocean gyres. *J. Mar. Res.*, **58,** 97–116.
Stammer, D., 1997: Global characteristics of ocean variability estimated from regional TOPEX/Poseidon altimeter measurements. *J. Phys. Oceanogr.*, **27,** 1743–1769.
——, 1998: On eddy characteristics, eddy transports, and mean flow properties. *J. Phys. Oceanogr.*, **28,** 727–739.
——, and C. Wunsch, 1999: Temporal changes in eddy energy of the oceans. *Deep-Sea Res.*, **46B,** 77–108.
Talley, L. D., 1983: Radiating instabilities of thin baroclinic jets. *J. Phys. Oceanogr.*, **13,** 2161–2181.
Treguier, A. M., and B. L. Hua, 1987: Oceanic quasi-geostrophic turbulence forced by stochastic wind fluctuations. *J. Phys. Oceanogr.*, **17,** 391–411.
——, and ——, 1988: Influence of bottom topography on stratified quasi-geostrophic turbulence in the ocean. *Geophys. Astrophys. Fluid Dyn.*, **43,** 265–305.
Vallis, G. K., 1983: On the predictability of quasi-geostrophic flow: The effects of beta and baroclinicity. *J. Atmos. Sci.*, **40,** 10–27.
Wardle, R. M., and J. S. Marshall, 2000: Representation of eddies in primitive equation models by a PV flux. *J. Phys. Oceanogr.*, **30,** 2481–2503.
Weatherly, G. L., and P. J. Martin, 1978: On the structure and dynamics of the oceanic bottom boundary layer. *J. Phys. Oceanogr.*, **8,** 557–570.
Willebrand, J., and Coauthors, 2001: Circulation characteristics in three eddy-permitting models of the North Atlantic. *Progress in Oceanography*, Vol. 48, Pergamon, 123–161.
Williams, G. P., and J. B. Robinson, 1974: Generalized Eady waves with Ekman pumping. *J. Atmos. Sci.*, **31,** 1768–1776.
Wunsch, C., 1997: The vertical partition of oceanic horizontal kinetic energy. *J. Phys. Oceanogr.*, **27,** 1770–1794.
——, 1998: The work done by the wind on the oceanic general circulation. *J. Phys. Oceanogr.*, **28,** 2332–2340.
——, 1999a: A summary of North Atlantic baroclinic variability. *J. Phys. Oceanogr.*, **29,** 3161–3166.
——, 1999b: Where do ocean eddy heat fluxes matter? *J. Geophys. Res.*, **104,** 13 235–13 249.
——, 2001: Ocean observations and the climate forecast problem. *Meteorology at the Millenium*, R. P. Pearce, Ed., Academic Press, 217–224.